

Journal of Biomedical Optics

SPIEDigitalLibrary.org/jbo

Quantitative phase microscopy of transparent samples using a liquid crystal display

Ignacio Iglesias
Fernando Vargas-Martin



SPIE

Quantitative phase microscopy of transparent samples using a liquid crystal display

Ignacio Iglesias and Fernando Vargas-Martin

Universidad de Murcia, Departamento de Física, Campus de Espinardo, E-30100, Murcia, Spain

Abstract. We propose a new quantitative phase microscope based on spatial filtering of the beam carrying the sample-induced wavefront. A prototype built using a transmissive liquid crystal display for the experimental demonstration of the principle and preliminary results obtained with artificial and biological samples are presented.

© The Authors. Published by SPIE under a Creative Commons Attribution 3.0 Unported License. Distribution or reproduction of this work in whole or in part requires full attribution of the original publication, including its DOI. [DOI: [10.1117/1.JBO.18.2.026015](https://doi.org/10.1117/1.JBO.18.2.026015)]

Keywords: microscopy; quantitative phase measurements.

Paper 12741R received Nov. 16, 2012; revised manuscript received Jan. 18, 2013; accepted for publication Jan. 21, 2013; published online Feb. 7, 2013.

1 Introduction

Transparency is a common property of living cells when observed by light microscopy in their natural or modified, but physiologically feasible, environments. Due to this property, only the phase is significantly modified by the sample, which complicates the noninvasive examination of cells and tissue of utmost importance in numerous fields of current biomedical research. Developmental biology, tissue engineering, optical tweezers, the control of laser ablation and laser micro-scalpels, cell migration and tissue changes in cancer research, membrane dynamics or cell motility studies are only some examples explaining why recent years have seen a steady increase in the number of new optical techniques for determining the tridimensional structure of microscopic transparent samples.¹⁻⁹

In this field, we recently introduced the pyramid phase microscopy (PPM),¹⁰ a nondiffractive and noninterferometric microscopy modality, which we believe has several advantages over others, the most significant being its low instrumentation complexity, its robustness against noise, mechanical stability, and the capability of real time imaging. Closely related with the Foucault knife-edge test, the technique is based on the splitting of the light by the use of a square base refractive pyramid¹¹ to sense the gradient of the wavefront on a given input plane. The pyramid is placed in the Fourier transform plane of the input plane that, in the PPM method, is the plane where the magnified image of the sample is formed after the tube lens of the microscope. Taking in to account the Fourier transform properties of lenses,¹² this image plane is brought to a position before a positive lens while the splitting is in the lens back focal plane.

Four independent spatially separate channels carrying the signals for the wavefront gradient determination are created after the focal plane by the following processes. Simultaneously to the splitting, the prism composing the pyramid incorporates different tilts in the divided beams that increase its separation with propagation. Once generated, the four beams are passed through additional optics that serve to re-image the input plane on to an image sensor as a charge coupled device (CCD). The four modified

images of the sample (or subimages) generated on the sensor are combined algebraically to produce, if a modulation is incorporated in the system,^{10,11,13} a conventional intensity image (such as the image that would have been obtained with a conventional microscope) and two images corresponding to the orthogonal components of the wavefront gradient.

Although diffraction scalar theory can be applied to rigorously demonstrate that the algebraic combination of the subimages is directly related with the input wavefront gradient,^{14,15} the more limited geometrical optics approach can also be used. Following this perspective, it can be shown^{10,11,13} that the pixels of the four subimages once grouped by the same associate input plane coordinates can be interpreted as the signals of an array of individual quad-cell detectors of the intersection positions of the rays with the focal plane. Taking into account that the rays are perpendicular to the wavefront in the input plane, a local average wavefront tilt will displace the intersection of the associated ray with the focal plane from the optical axis an amount proportional to the tilt magnitude. As a consequence, the positions coordinates calculated from the array of quad-cell signals can be also interpreted as proportional to the values of the orthogonal components of the local gradient on the input plane.

2 PPM by Fourier Plane Filtering

As can be expected, the pyramid technique for quantitative phase microscopy also has its limitations. An obvious one is that the four images of the sample must be accommodated in the CCD sensor area. For this reason, the PPM provides images with gradient information but of reduced transversal resolution or restricted image field compared with the image obtained using a conventional microscope with equivalent optics and image sensor. Another potential difficulty for its general use might be the availability of a nonstandard optical element (e.g., the glass pyramid) of sufficient quality in terms of planarity, equality of the angles between the faces, and sharpness of the edges. We should mention that a recent proposal involves implementation of the PPM using a squared array of four lenses¹⁶ integrating the splitting with the reimaging optics in a single refractive component, which translates the requirements for the optical quality of the pyramid to the optical quality of a

Address all correspondence to: Ignacio Iglesias, Universidad de Murcia, Departamento de Física, Campus de Espinardo, E-30100, Murcia, Spain. E-mail: iic@um.es

nonstandard component with the same limitations in terms of lateral resolution.

However, as we propose here, the spatial separation of channels and the pyramid itself—or other nonconventional optical components—can be avoided if time multiplexing is considered, using a single spatial channel (the common conventional-microscope light path) combined with the blocking of the beam at the back focal plane or, in other words, the sequential spatial frequency filtering of the input wavefront spectrum.

We will show that this can be easily implemented by using an optoelectronic device such as a liquid crystal operating as an intensity modulator to block the light in a Fourier transforming plane.

3 Experimental System

The setup developing this idea using a liquid crystal display (LCD) (Panasonic, P13SM014, 800 × 600 pixels) extracted from a commercial video projector is shown in Fig. 1(a). One important characteristics of the above-described gradient sensor is its saturation even for small wavefront local tilts without modulation. To broad the range to a useful interval, we implement the previously reported strategy¹⁰ of modulate the sensor using for illumination an incoherent symmetrical planar source that illuminates the sample from infinite. To form this source, a white led, L, (Osram, Golden Dragon LW W55M

5600 K) with the encapsulation optics removed, is collimated and passed through a ground glass diffuser, D, to form an extended uniform source of 10.5 Ø mm diameter. The diffuser is placed on the front focal plane of a lens, L1 (all the lenses in the system are doublet acromats), at its exit pupil, a distribution of simultaneous illumination directions all incoherent with each other. Given that, by technical reasons the sample cannot be directly placed on this plane, it is transported to the sample plane by means of a relay system composed of equal lenses L2 and L3 arranged as an afocal system with unit magnification. The sample, S, is placed on a micrometric translation stage that allows lateral and axial positioning. A microscope consisting of an objective, MO, (Nikon, CFI PF ELWD DM 40x NA 0.60) and a tube lens, L4, is placed behind. The lens L4 forms a scaled copy of the sample-generated light field at a focal distance of the lens L5. At an additional distance in the direction of the light propagation, the LCD is placed on a three-axis micrometric translation stage. Finally, the lens L6 images the sample on a CCD camera (Andor Ixon, 512 × 512 pixels 16 × 16 µm pixel size). The lateral position of the LCD is adjusted without the sample inserting a lens, L7 [drawn in the scheme of Fig. 1(a) with a dotted line], to focus on the CCD the spot on the LCD. After ensuring that it becomes equally occluded by the displayed patterns, the lens L7 is removed.

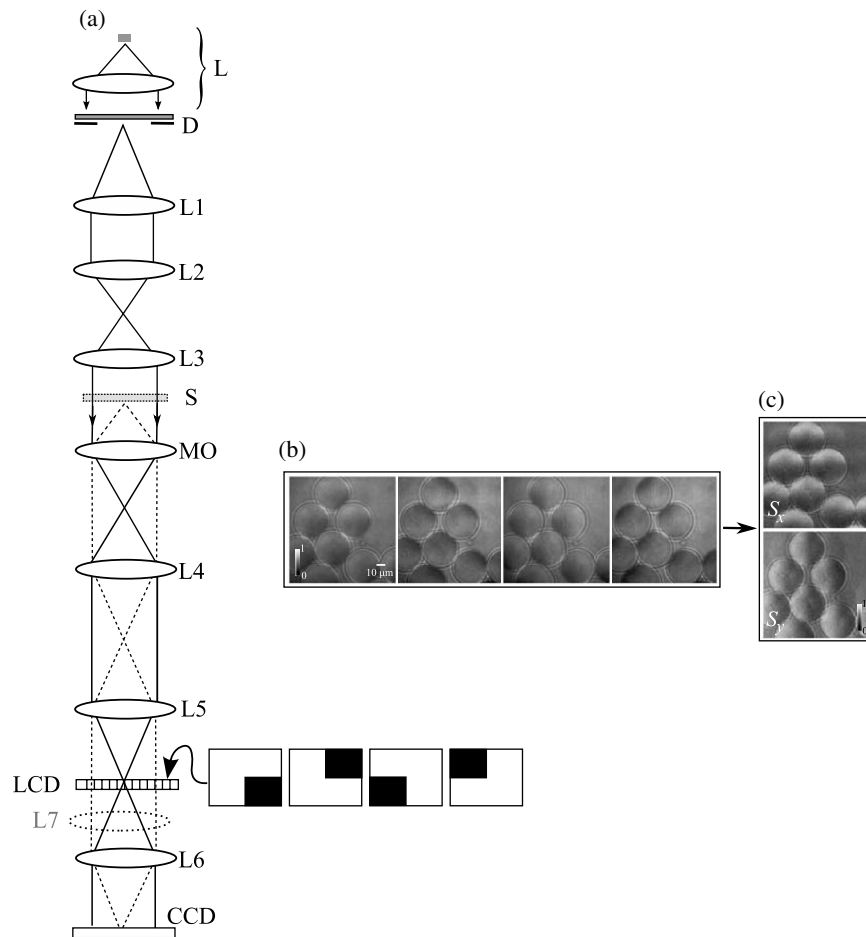


Fig. 1 (a) Experimental setup for quantitative phase microscopy using a liquid crystal display: L collimated led beam; D, diffuser; A, aperture; L1-L3, lenses; S, sample; MO, microscope objective; L4, tube lens; L5, lens; LCD, liquid crystal display; L6 lens; L7 lens; CCD camera. In the inset, the binary patterns (black means that the light is blocked, white the opposite) sequentially displayed in the LCD. The acquired images and the gradient information obtained from them; (b) a sample set of the images corresponding to the binary patterns shown in (a); (c) the gradients in orthogonal directions computed using Eq. (1). All images have 512 × 512 pixels.

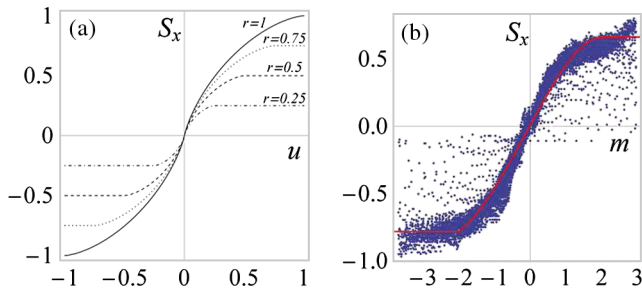


Fig. 2 Sensor calibration: (a) expected response normalized using an incoherent disc source for different radii; (b) plot of the signals (blue dots) versus slope and the fit (red curve) used to linearize the sensor response.

The binary patterns displayed in the LCD are shown in the inset of Fig. 1(a). Each of them is used sequentially to acquire the set of images, I_i , whose sum is the conventional microscope image, I , of the sample amplitude absorption map. Similarly to the PPM, pixel-by-pixel signals, S_x and S_y , proportional to the gradients in the x and y directions, are obtained by computing

$$\begin{bmatrix} S_x \\ S_y \end{bmatrix} = \frac{1}{I} \begin{bmatrix} I_1 + I_2 - I_3 - I_4 \\ I_1 + I_3 - I_2 - I_4 \end{bmatrix}. \quad (1)$$

Note that, unlike in the PPM, in which a pyramid face selects a quadrant, a quadrant is sequentially filtered out. It can be easily demonstrated that the signals in Eq. (1) are inverted with respect

to the PPM signals. Although the negative version of the filter set is also possible, less light would be gathered, with a consequent reduction in the signal-to-noise ratio.

4 Experimental Results

To test the system, we first used polystyrene ($n_F^* = 1.60$) microspheres of diameter $d = 43.3 \mu\text{m}$ \varnothing (Polybead, Polysciences) immersed in a calibrated liquid with a refractive index of $n_F^h = 1.56$ (Cargille Labs) to simulate the cell-medium index mismatch inside a sealed chamber formed by a microscope slide and a cover slip separated by spacers. A sample of the images obtained for each pattern is shown in Fig. 1(b). Figure 1(c) shows the images resulting from the calculation of Eq. (1) over that set.

The extended source illumination generates a sensor gain curve that depends on the area.¹⁰ Using geometrical optics, it can be easily shown that, for a perfect annular incoherent source of radius r , the ideal response, S_u , for a given local wavefront tilt at a certain transversal coordinates in the input plane is proportional to

$$S_u = \begin{cases} -r & u \leq -r \\ (2r/\pi)\sin^{-1}u/r & -r < u < r \\ r & u \geq r \end{cases}, \quad (2)$$

where u represents the x or y (normalized with respect to r) position coordinates of the ray intersection with the lens back focal plane. The expected response of a uniform illumination diffuser,

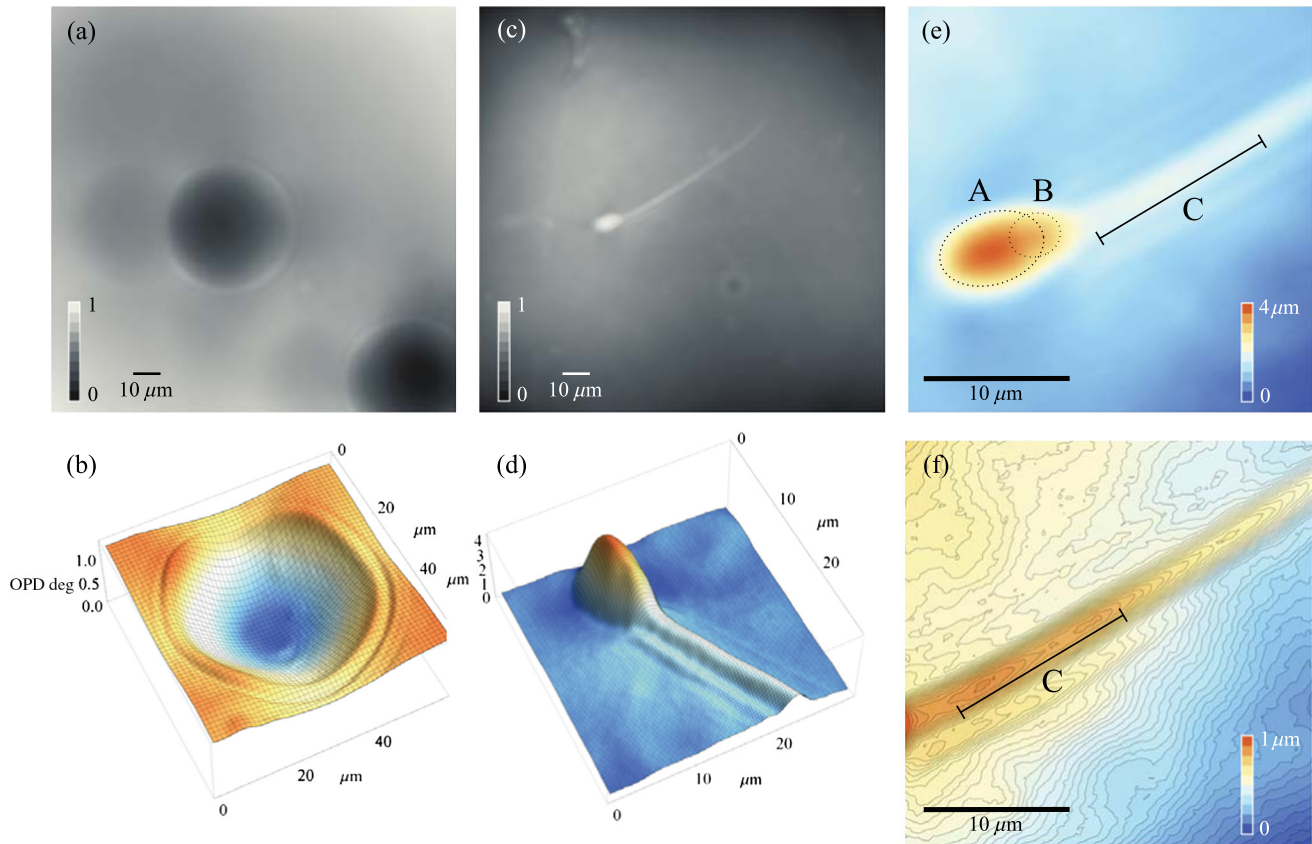


Fig. 3 Experimental result of polystyrene microspheres and a fixed sperm cell sample: (a) normalized representation (512 × 512 pixels) of the phase generated by the sample of microspheres; (b) detail of the central microsphere represented in radians of OPD; (c) normalized representation of the reverse phase generated by a porcine spermatozoon; (d) detail of the head (50 × 50 pixels) represented as a tridimensional height map; (e) the same detail with some morphological characteristics labeled; (f) the same window (50 × 50 pixels) displaced to show the sperm tail.

can be obtained by integration of the Eq. (2). Figure 2(a) shows this, and also how the gain is modified and the sensor becomes saturated earlier when the source radius decreases.

In a real system, the response can be affected by not completely known or controllable factors such as the scattering parameters of the diffuser. A safe way to proceed is to calibrate the sensor with a known sample. The blue dots in Fig. 2(b) represent the entire set of local gradient signals in the acquired image corresponding to the x -direction versus the slope, $m = \tan(\theta)$, generated in the wavefront by a single microsphere such as the one appearing in Fig. 1(b). These values are used to find a gain curve (red line) by fitting to a piecewise function consisting of a four-degree polynomial and two saturation constants. The numerous data points ensure consistent estimation of the response even in the presence of noise or artefacts. It can be observed that the response of our experimental setup follows the expected gain of Fig. 2(a) and that the sensor becomes saturated at an angle of approximately $\theta = 64$ deg, which is directly related with the radius of the extended illumination source on the Fourier plane.

As is apparent in the images in Fig. 1(b) and 1(c), an artefact emerges in the form of spurious object replicas corresponding with the first diffraction orders of the matrix pixelated arrangement of the LCD undesirable behaving as a square grating.

Also in the images, ringed artefacts caused by diffraction can be observed. At the rim, the microsphere acts as an annular mask, given that the high spatial frequency propagation vectors generated there by the extremely high interphase surface gradient are filtered out by the microscope optics. Regions with similar topological characteristics to these will induce similar diffraction artefacts in other samples, as can be observed below.

Figure 3(a) shows the retardation map obtained using the linearized-response version of the images obtained after using Eq. (1) as input of a Frankot-Chellapa¹⁷ integration algorithm. Figure 3(b) shows a tridimensional retardation map of the central sphere. The scale of the height axis is obtained using $\lambda_F = 486$ nm (the F-line is close to the peak value of the diode spectrum) and the maximum retardation the microsphere generates ($2\pi d/\lambda_F)(n_F^s - n_F^h)$ along its symmetry axis.

In order to confirm that the prototype can resolve real biological samples, preparations of porcine (*Sus scrofa*) spermatozoa were used. Sperm cells in liquid present almost perfect refractive index matching, making these samples completely transparent. For this reason, they are routinely studied using conventional phase contrast techniques, which only provide partial information. Quantitative phase microscopy is especially interesting for studying these cells, as mentioned in Ref. 18.

The samples were prepared after fixation with 1% formaldehyde solution in phosphate buffered saline (PBS). The viscosity of the solution was increased using an additive (Bindobin; Tartex & Dr Ritter) (5 mg/mL).¹⁹ A drop (7 μ L) of the sperm suspension was placed between a glass slide and a cover slip (24 \times 24 mm). Figure 3(c) shows an example of the acquired images presented as a normalized thickness map. Assuming, for simplicity (the refraction index mismatch between the cell and the medium was unknown), that the maximum diameter of the sperm head is 4 μ m (Ref. 20), a height map can be drawn as shown in Fig. 3(d). Figure 3(e) shows how the sperm head appears to be composed of two intersecting ellipsoids labeled as A and B corresponding with the acrosomal and postacrosomal regions. In the tail, see the contour plot in Fig. 3(f), a segment of higher diameter, labeled as C, can be identified as the middle piece corresponding with the mitochondrial sheath.

5 Conclusions

To conclude, we have shown that quantitative phase microscopy can be easily carried out by filtering the microscopic sample-altered wavefront in a Fourier transformation plane after the tube lens of a conventional microscope. This new technique shares most of the virtues of PPM, but the optical system complexity is further reduced by substituting the glass pyramid by a simpler component.

The optical bench demonstration microscope used a transmissive LCD for the spatial filtering. Even though this device is not designed for this application and introduced unwanted artifacts, the prototype resolves submicron cellular structures in transparent biological samples. Improved image quality can be easily attained using a custom made liquid crystal, or another device, such as an actuatable mirror, with four uniform segments for sequential blocking of the beam.

The technique provides higher efficiency in the use of light given that, for the same sample-illumination intensity, time multiplexing provides three times more photons per subimage than the generation of four spatially separated channels. This characteristic can be useful to minimize photo-damage or to reduce the exposure time. If the last alternative is exploited, our proposed technique will allow the real-time imaging of microscopic phase changes by combining rapid acquisition with a fast optoelectronic beam-blocking device.

Acknowledgments

The authors thank Joaquín Gadea from the Departamento de Fisiología of the Universidad de Murcia for helpful discussions and in the preparation of the biological samples. I.I. acknowledges support from the Spanish Ministerio de Economía y Competitividad, grant DPI2012-32994.

References

1. M. R. Amison et al., "Linear phase imaging using differential interference contrast microscopy," *J. Microsc.* **214**(1), 7–12 (2004).
2. S. Bernet et al., "Quantitative imaging of complex samples by spiral phase contrast microscopy," *Opt. Express* **14**(9), 3792–3805 (2006).
3. F. Charrière et al., "Cell refractive index tomography by digital holographic microscopy," *Opt. Lett.* **31**(2), 178–180 (2006).
4. P. Bon et al., "Quadriwave lateral shearing interferometry for quantitative phase microscopy of living cells," *Opt. Express* **17**(15), 13080–13094 (2009).
5. D. Fu et al., "Quantitative DIC microscopy using an off-axis self-interference approach," *Opt. Lett.* **35**(14), 2370–2372 (2010).
6. S. S. Kou et al., "Transport-of-intensity approach to differential interference contrast (TI-DIC) microscopy for quantitative phase imaging," *Opt. Lett.* **35**(3), 447–449 (2010).
7. T. Kim and G. Popescu, "Laplace field microscopy for label-free imaging of dynamic biological structures," *Opt. Lett.* **36**(23), 4704–4706 (2011).
8. T. Kim, S. Sridharan, and G. Popescu, "Gradient field microscopy of unstained specimens," *Opt. Express* **20**(6), 6737–6745 (2012).
9. M. Martínez-Corral and G. Saavedra, "The resolution challenge in 3D optical microscopy," in *Progress in Optics*, E. Wolf, Ed., pp. 1–67, Elsevier, The Netherlands (2009).
10. I. Iglesias, "Pyramid phase microscopy," *Opt. Lett.* **36**(18), 3636–3638 (2011).
11. R. Ragazzoni, "Pupil plane wavefront sensing with an oscillating prism," *J. Mod. Opt.* **43**(2), 289–293 (1996).
12. J. W. Goodman, *Fourier Optics*, pp. 101–107, McGraw-Hill, New York (1996).
13. I. Iglesias et al., "Extended source pyramid wave-front sensor for the human eye," *Opt. Express* **10**(9), 419–428 (2002).
14. E. H. Linfoot, "On the Interpretation of the Foucault Test," *Proc. R. Soc. Lond. A Math. Phys. Sci.* **193**(1033), 248–259 (1948).

15. C. Véraud, "On the nature of the measurements provided by a pyramid wave-front sensor," *Opt. Commun.* **233**(1–3), 27–38 (2004).
16. A. B. Parthasarathy et al., "Quantitative phase imaging using a partitioned detection aperture," *Opt. Lett.* **37**(19), 4062–4064 (2012).
17. R. T. Frankot and R. Chellappa, "A method for enforcing integrability in shape from shading algorithm," *IEEE Trans. Pattern Anal. Mach. Intell.* **10**(4), 439–451 (1988).
18. P. Memmolo et al., "Identification of bovine sperm head for morphometry analysis in quantitative phase-contrast holographic microscopy," *Opt. Express* **19**(23), 23215–23226 (2009).
19. P. Coy et al., "Differing sperm ability to penetrate the oocyte *in vivo* and *in vitro* as revealed using colloidal preparations," *Theriogenology* **72**(9), 1171–1179 (2009).
20. M. C. Gil et al., "Morphometry of porcine spermatozoa and its functional significance in relation with the motility parameters in fresh semen," *Theriogenology* **71**(2), 254–263 (2009).